Available online at www.sciencedirect.com
ScienceDirect
Journal of Sound and Vibration 307 (2007) 564–577
JOURNAL OF SOUND AND VIBRATION
www.elsevier.com/locate/jsvi

Computing reflection and transmission coefficients for plate reinforcement beams

J.R.F. Arruda[a,*], F. Gautier[b], L.V. Donadon[a]

[a]*Laboratório de Vibroacústica, Faculdade de Engenharia Mecânica, Universidade Estadual de Campinas, Rua Mendeleiev, 200 Cidade Universitária, Caixa postal 6122, CEP 13083-970, Campinas, SP, Brazil*
[b]*Laboratoire d'Acoustique, Université du Maine, Avenue Olivier Messiaen, 72085 Le Mans, France*

Received 20 December 2004; received in revised form 17 May 2006; accepted 13 June 2007
Available online 4 September 2007

Abstract

In this paper, we investigate the possibility of obtaining experimentally the reflection and transmission coefficients for propagating bending waves in infinite thin plates caused by a reinforcing beam that is flexibly connected to the plate. A reinforced plate spectral element including the attachment flexibility effect was derived and implemented computationally for this purpose. The proposed technique was numerically verified by using a system consisting of a long simply supported rectangular plate wave-guide. The system was modeled using the derived spectral element, which was validated by comparison with a finite element model. The dynamic responses simulated at a few locations are used to compute the reflection and transmission coefficients. Theoretical expressions of the reflection and transmission coefficients were obtained by using a transfer matrix formulation for the plate and for the flexibly connected beam. The coefficients obtained by using the proposed method are compared with the theoretical values and good agreement is found. The proposed numerical model can be used to optimize the experimental conditions for extracting the reflection and transmission coefficients. The reflection and transmission coefficients obtained with the proposed technique can be used, for instance, in ray-tracing methods, which are currently under development.

1. Introduction

Modal methods are widely used to predict the vibratory behavior of assembled structures such as stiffened panels. However, the increase of the modal density with frequency limits the use of such methods to the low-frequency range. For high frequencies, the statistical energy analysis (SEA) method provides an estimation of frequency- and space-averaged vibratory levels for each sub-system [1]. However, the strong assumptions necessary to the application of SEA and the accuracy of its predictions are not easy to evaluate *a priori*. Ray-tracing methods, also called image methods, are alternative methods in which the vibratory field is represented by plane waves propagating in every direction [2]. Interactions of the incident waves with the boundaries of

*Corresponding author. Tel.: +55 19 3521 3194; fax: +55 19 3289 3722.
E-mail addresses: arruda@fem.unicamp.br (J.R.F. Arruda), francois.gautier@univ-lemans.fr (F. Gautier), lazaro@fem.unicamp.br (L.V. Donadon).

0022-460X/$ - see front matter © 2007 Elsevier Ltd. All rights reserved.
doi:10.1016/j.jsv.2007.06.052

each sub-structure lead to reflected and transmitted fields, like in a billiard game. In this approach, reflection and transmission coefficients are the key parameters for the system modeling.

For flat panels reinforced with beams, various models of these coefficients have been developed. A reference configuration consists of an infinite plate reinforced by two infinite beams placed symmetrically with respect to the middle surface of the plate. Assuming Kirchhoff's model for the plate, Euler–Bernoulli's model for the beam, and rigid beam/plate connection, Cremer, [3], Heckl [4] and Ungar [5] have determined reflected and transmitted fields resulting from an incident bending wave. This model has been used for active attenuation of a plate flexural wave transmission [6]. Using a more general state vector formalism, these coefficients have been determined by Kouzov [7], assuming that the reinforcing beam is modeled as a thin plate of finite width rigidly connected to the plate.

A great number of stiffener models have been developed in the literature. However, they are often developed to compute the plate response to acoustical or mechanical excitation, and the attention is generally not focused on reflection and transmission coefficients. However, a short list of illustrative analytical models of stiffeners can be drawn. They are based on assumptions related to the reinforcement itself (usually consisting of a beam of complex cross-section), to the plate's model and to the connection condition between the two.

Orthogonal sets of stiffeners placed on a plate can be taken into account in a global way by using the grillage method as presented by Balendra and Shanmugam [8]. In this case, mechanical characteristics (density and bending stiffness) of an equivalent orthotropic plate are determined in an approximate way. A simple model of stiffener has been developed by Mead [9] for estimating the response of a periodic ribbed plate. The plate is supposed to be supported elastically along parallel line supports describing the stiffeners. Each stiffener is modelled as a line of rotationnal and translational springs. Another elementary rib model is presented by Keltie [10]. In this study, stiffener is supposed to provide only purely inertial reaction and the added stiffness added by the beam is ignored. Making use of the spatial Fourier transform, it is shown [11] that a reinforcement placed on a plate generates both equivalent shear forces and equivalent bending moments. These excitation sources are present in the right-hand term of the equation of motion of the plate and are determined using the continuity conditions and the equations of motion of the stiffener itself. In this case, the stiffener is generally modelled using a beam equation. For rigid beam/plate connection, this kind of approach is applied in Ref. [12] assuming that equivalent forces act only on the plate, and in Ref. [13] assuming that both equivalent forces and moments are acting on the plate. Such approach is well adapted and widely used to model periodic ribbed structures (see [14] for a review). If the beam stiffener has no symmetry with respect to the neutral plane of the plate, coupling between out-of-plane and in-plane coupling occurs, i.e., an incident flexural wave can induce longitudinal waves in the plate. A complete set of stiffener's equations based on the theory of complex cross-section beams is presented by Langley and Heron [15]. It includes out- and in-plane displacements in the plate and in the beam and takes into account shear deformation, rotary inertia and warping of the beam cross-section. The connection between plate and beam can be modeled using 3D elasticity. The case of a Midlin's plate with symmetric stiffeners is presented in Ref. [16] by Zalizniak, Tsoa and Wood.

Besides in-plane and out-of-plane wave coupling, the elasticity of the connection between the plate and the stiffener beam is another important characteristic of junctions. In practice, the reinforcing beam can be welded or fixed on the plate using screws, rivets or glue. Such technical realizations induce a flexibility of the connection between the two substructures. The exact conditions of the connection between the two are often not well known and can vary in an important way, leading to an important scattering of the vibratory response. Uncertainties on the connection characteristics are, in practice, a major source of discrepancies between numerical predictions and measurements. Measurements and experimental characterization of flexible joints appear much less in the literature than analytical or numerical models. However, experimental values and models of equivalent stiffness of junctions would be very useful, since they are very difficult to model. Experimental methods have been developed for measuring reflection and transmission coefficients for bending waves in beams by Pavic [17] and by Feng [18]. The case of coupled longitudinal and flexural motion and the case of dissipative junctions are presented by Gautier and Moulet [19]. This kind of measurement has not been extended to 2D configurations, such as stiffened plates.

This last point provides the motivation for the present analysis, in which the authors investigate the possibility of experimentally obtaining reflection and transmission coefficients for propagating bending waves

in infinite thin plates caused by a reinforcing beam that is flexibly connected to the plate. For this purpose, and in order to reduce the amount of algebra, a spectral element formulation, as presented by Doyle in Ref. [20], is used to compute simulated responses of a measurement configuration. After the introduction, the spectral element method is used in Section 2 to model the structural discontinuity constituted by the reinforcing beam elastically connected to the plate. Validation of the proposed spectral element is provided in Section 3 using comparisons with the finite element method. Theoretical reflection and transmission coefficients are presented in Section 4. The proposed measurement method and its numerical simulation are provided in Section 5.

2. Spectral element formulation

Starting with the Kirchhoff plate equation,

$$D\nabla^2\nabla^2 w(x,y) - \omega^2\rho h w(x,y) = F(x,y), \tag{1}$$

where $D = Eh^3/12(1-\upsilon)^2$, h is the thickness, υ is the Poisson ratio, ρ is the density, and $w(x,y)$ represents the transverse displacement of the plate. Assuming a boundary condition in one direction, say the y direction, the solution along the orthogonal direction x is written in terms of propagating waves [21]. When the plate is simply supported along two parallel sides, assuming a sinusoidal solution along y, the transverse displacement can be written as

$$w(x,y) = \sum_{n=1}^{N} \left[A_n e^{-ik_{1n}x} + B_n e^{ik_{1n}x} + C_n e^{-k_{2n}x} + D_n e^{k_{2n}x}\right] \sin(k_{yn}y). \tag{2}$$

The wavenumbers can be computed by replacing Eq. (2) in Eq. (1), and using the following properties of the sine function: $d^2\sin(k_{yn}y)/dy^2 = -k_{yn}^2\sin(k_{yn}y)$ and $d^4\sin(k_{yn}y)/dy^4 = k_{yn}^4\sin(k_{yn}y)$. It is important to mention here that these properties are essential in developing the method, and they only hold for the simply supported plate. For other boundary conditions, the solution along the y direction involves a sum of trigonometric and hyperbolic functions on y and, thus, these properties do not hold for the full solution. This is a limiting factor for extending this approach to other boundary conditions, which involve odd order derivatives. Nevertheless, approximate solutions, where the hyperbolic functions are developed in Fourier series can be developed [22] for other boundary conditions.

The wavenumbers are given by

$$k_{1n} = \sqrt{k_p^2 - k_{yn}^2},\ k_{2n} = \sqrt{k_p^2 + k_{yn}^2},\ k_p = (\omega^2\rho h/D)^{1/4} \quad \text{and} \quad k_{yn} = n\pi/L_y. \tag{3}$$

The coefficients A_n, B_n, C_n and D_n are found using the transverse and angular displacements at the two ends as boundary conditions, and using the moment and effective shear force expressions [20]:

$$M_x = D\left[\frac{\partial^2 w}{\partial x^2} + \upsilon\frac{\partial^2 w}{\partial y^2}\right] \quad \text{and} \quad V_x = Q_x + \frac{\partial M_{xy}}{\partial y} = -D\left[\frac{\partial^3 w}{\partial x^3} + (2-\upsilon)\frac{\partial^3 w}{\partial x \partial y^2}\right]. \tag{4}$$

One may look at the proposed solution to the wave equation as a wave propagation solution in the x direction and by a sum of sine functions in the y direction. This sine terms can be interpreted as propagation modes. Each mode n will only propagate for frequencies that are higher than the frequency where the wavenumber associated to it, k_{1n} in Eq. (3), becomes real, i.e., $k_p \geqslant k_{yn}$. Given a desired frequency range, it is then straightforward to determine how many propagation modes, N, should be taken into account.

The thin plate spectral element matrix can be obtained by writing the shear force and the moment using the displacements and the slopes at the two extremities along x. Considering an element with

length L_x in the x dimension, the transverse displacement and the slope at positions $x=0$ and L_x are given by

$$\frac{1}{\sin(k_y y)}\begin{Bmatrix} w_1 \\ \phi_1 \\ w_2 \\ \phi_2 \end{Bmatrix} = \begin{bmatrix} 1 & 1 & 1 & 1 \\ -\mathrm{i}k_1 & \mathrm{i}k_1 & -k_2 & k_2 \\ \mathrm{e}^{-\mathrm{i}k_1 L_x} & \mathrm{e}^{\mathrm{i}k_1 L_x} & \mathrm{e}^{-k_2 L_x} & \mathrm{e}^{k_2 L_x} \\ -\mathrm{i}k_1 \mathrm{e}^{-\mathrm{i}k_1 L_x} & \mathrm{i}k_1 \mathrm{e}^{\mathrm{i}k_1 L_x} & -k_2 \mathrm{e}^{-k_2 L_x} & k_2 \mathrm{e}^{k_2 L_x} \end{bmatrix} \begin{Bmatrix} A \\ B \\ C \\ D \end{Bmatrix} = [\alpha] \begin{Bmatrix} A \\ B \\ C \\ D \end{Bmatrix}, \tag{5}$$

where $\phi = \mathrm{d}w/\mathrm{d}x$.

And the shear force and the moment are given by

$$\frac{1}{\sin(k_y y)}\begin{Bmatrix} V_1 \\ M_1 \\ V_2 \\ M_2 \end{Bmatrix} = D \begin{bmatrix} \alpha_1 & -\alpha_1 & \alpha_2 & -\alpha_2 \\ \beta_1 & \beta_1 & \beta_2 & \beta_2 \\ -\alpha_1 \mathrm{e}^{-\mathrm{i}k_1 L_x} & \alpha_1 \mathrm{e}^{\mathrm{i}k_1 L_x} & -\alpha_2 \mathrm{e}^{-k_2 L_x} & \alpha_2 \mathrm{e}^{k_2 L_x} \\ -\beta_1 \mathrm{e}^{-\mathrm{i}k_1 L_x} & -\beta_1 \mathrm{e}^{\mathrm{i}k_1 L_x} & -\beta_2 \mathrm{e}^{-k_2 L_x} & -\beta_2 \mathrm{e}^{k_2 L_x} \end{bmatrix} \begin{Bmatrix} A \\ B \\ C \\ D \end{Bmatrix} = [\beta] \begin{Bmatrix} A \\ B \\ C \\ D \end{Bmatrix}, \tag{6}$$

where

$$\alpha_1 = \mathrm{i}k_1^3 + \mathrm{i}k_y^2(2-\upsilon)k_1;\ \alpha_2 = -k_2^3 + k_y^2(2-\upsilon)k_2;\ \beta_1 = k_1^2 + \upsilon k_y^2;\ \beta_2 = -k_2^2 + \upsilon k_y^2 \tag{7}$$

and the subscript n was dropped for simplicity. Thus, combining the equations above to write the element matrix gives

$$\{\, V_1 \quad M_1 \quad V_2 \quad M_2 \,\}^{\mathrm{T}} = [\beta][\alpha]^{-1}\{\, w_1 \quad \phi_1 \quad w_2 \quad \phi_2 \,\}^{\mathrm{T}} = [K]\{\, w_1 \quad \phi_1 \quad w_2 \quad \phi_2 \,\}^{\mathrm{T}}. \tag{8}$$

It is interesting to note that the element matrix is independent of the term $\sin(k_{yn}y)$ and the sum in k_{yn} can be performed for each element independently, or it can be done after the global matrix assembled. In order to complete the process, the force must be projected on the basis of sine function in terms of k_{yn} related to the y direction. This representation takes into account the position of the concentrated driving force, y_0, and it is given by

$$F_n = F_0 \frac{2}{L_y} \sin(k_{yn} y_0). \tag{9}$$

The final solution will be given by the sum in the y direction expressed in Eq. (2), which can be interpreted as a propagation mode superposition. The global matrix is assembled with the standard direct stiffness method [23].

2.1. Introducing the beam reinforcements on the plate element

Stiffener beams can be introduced in the Spectral element model plate element. If they are assumed to be ideally attached to the plate [4], the effective shear force and the bending moments at the end of the plate will

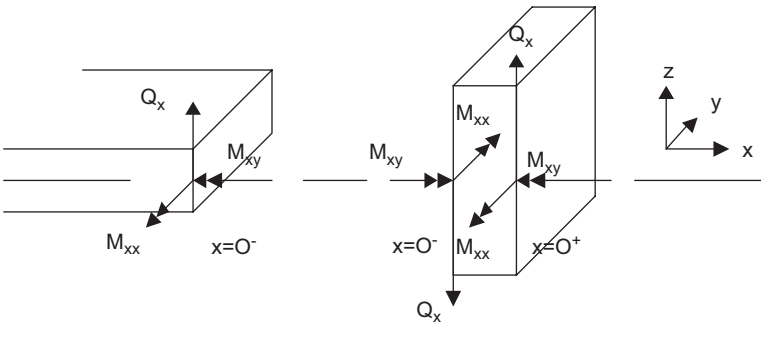

Fig. 1. Equilibrium for a plate with an edge rigidly connected to a beam.

be equal to those in the beam, as shown in Fig. 1, and the equations of motion become

$$EI_b \frac{\partial^4 u(y)}{\partial y^4} - \omega^2 \rho A u(y) = \left(Q_x + \frac{\partial M_{xy}}{\partial y} \right)_{x=O^-} - \left(Q_x + \frac{\partial M_{xy}}{\partial y} \right)_{x=O^+}, \tag{10}$$

$$GJ_b \frac{\partial^2 \theta(y)}{\partial y^2} + \omega^2 \rho I_p \theta(y) = (M_{xx})_{x=O^-} - (M_{xx})_{x=O^+}, \tag{11}$$

where $u(y)$ is the transverse displacement of the beam, $\theta(y)$ is the torsion angle of the beam, EI_b and GJ_b are the flexural and torsional rigidity of the beam, respectively, and ρA, ρI_p are the mass and the polar mass moment of inertia per unit length of the beam, respectively. Note that, when the flexural waves reach the beam, they introduce both flexural and torsional motion in the beam.

Thus, modified boundary condition can be established at position $x = O^+$ to take into account the effective shear force and the moment including the beam effects as

$$V_x = -D\left[\frac{\partial^3 w}{\partial x^3} + (2-\upsilon) \frac{\partial^3 w}{\partial x \partial y^2} \right] + EI_b \frac{\partial^4 w}{\partial y^4} - \omega^2 \rho A w, \tag{12}$$

$$M_x = D\left[\frac{\partial^2 w}{\partial x^2} + \upsilon \frac{\partial^2 w}{\partial y^2} \right] - GJ_b \frac{\partial^3 w}{\partial x \partial y^2} - \omega^2 \rho I_p \frac{\partial w}{\partial x}. \tag{13}$$

The beam effect in the boundary conditions must be applied at the position of the stiffener. Here, the stiffener will be placed at one edge of the spectral plate element. Using the same procedure used to derive Eq. (6), the modified matrix $[\beta_n]$ can be obtained:

$$[\beta_n] = D \begin{bmatrix} \alpha_1 & -\alpha_1 & \alpha_2 & -\alpha_2 \\ \beta_1 & \beta_1 & \beta_2 & \beta_2 \\ \left(-\alpha_1 + \frac{\delta_1}{D}\right) e^{-ik_1 L_x} & \left(\alpha_1 + \frac{\delta_1}{D}\right) e^{ik_1 L_x} & \left(-\alpha_2 + \frac{\delta_1}{D}\right) e^{-k_2 L_x} & \left(\alpha_2 + \frac{\delta_1}{D}\right) e^{k_2 L_x} \\ \left(-\beta_1 - i\frac{\delta_2}{D} k_1\right) e^{-ik_1 L_x} & \left(-\beta_1 + i\frac{\delta_2}{D} k_1\right) e^{ik_1 L_x} & \left(-\beta_2 - \frac{\delta_2}{D} k_2\right) e^{-k_2 L_x} & \left(-\beta_2 + \frac{\delta_2}{D} k_2\right) e^{k_2 L_x} \end{bmatrix}, \tag{14}$$

where the modifying terms are

$$\delta_1 = EI_b k_y^4 - \omega^2 \rho A; \; \delta_2 = GJ_b k_y^2 - \omega^2 \rho I_p. \tag{15}$$

Another form of including the stiffener in the spectral element formulation is using its transfer matrix. If we take into account the elasticity of the beam/plate connection, the transfer matrix of a symmetric stiffener such

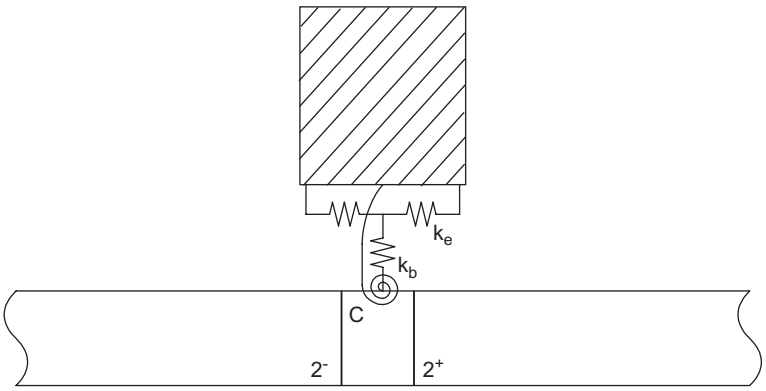

Fig. 2. Reinforcement beam with flexible connection to the plate.

as shown in Fig. 2 is given by [19]

$$T(2^+,2^-)=\begin{Bmatrix} w\\ \phi\\ V\\ M\end{Bmatrix}_{2^+}=\begin{bmatrix}1&0&0&0\\0&1&0&0\\ \delta_1&0&1&0\\0&\delta_2&0&1\end{bmatrix}\begin{Bmatrix} w\\ \phi\\ V\\ M\end{Bmatrix}_{2^-}, \tag{16}$$

where the points 2^- and 2^+ are indicated in Figs. 2 and 3 and

$$\begin{aligned}\delta_1&=2\left(E(I_b+\alpha A z_G^2)k_y^4-\frac{\omega^2\rho A}{1-\omega^2\rho A/k_b}\right),\\ \delta_2&=2\left\{\frac{GJ_bk_y^2-\omega^2\rho I_p}{(C+GJ_bk_y^2-\omega^2\rho I_p)}\left[C+\omega^2\rho A\left(z_G-\frac{h}{2}\right)\frac{\Delta_2}{\Delta_1}\right]-\omega^2\rho A z_G\frac{\Delta_2}{\Delta_1}\right\},\end{aligned} \tag{17}$$

where

$$\Delta_1=1-\frac{\omega^2\rho A}{k_e}-\frac{(z_G-(h/2))^2\omega^2\rho A}{C+GJ_bk_y^2-\omega^2\rho I_p},\quad \Delta_2=\frac{h}{2}+\frac{C(z_G-(h/2))}{C+GJ_bk_y^2-\omega^2\rho I_p}. \tag{18}$$

Parameters k_b and k_e are the stiffness per unit length associated to translational springs in the out-of plane (z) an in-plane (x) direction, respectively. Parameter C denotes the torsional stiffness per unit length describing the elasticity of the connection. In Eq. (17), a correction term α was included. As the connection between the plate and the beam is not rigid in the z direction, the neutral axis position for the beam will no longer be the neutral plane of the plate. When the stiffness coefficient k_e goes to infinity, α goes to 1, while, when k_e goes to 0, α also goes to 0, as each beam will then have its neutral line passing through its own centroid. Note that all derivations were made for two identical beams placed on either side of the plate with the same connection flexibility. For simplicity, only one beam and its connection to the plate is represented on Fig. 2.

In order to include the effects of the changes in the shear force and in the bending moment due to the stiffener, it is considered one spectral element, as defined in Fig. 3.

The dynamic stiffness matrix of the element was shown in Eq. (8) to be given by $[K][\beta][\alpha]^{-1}$, which can be written as

$$\begin{Bmatrix}V_1\\M_1\\V_2\\M_2\end{Bmatrix}=[K]\begin{Bmatrix}w_1\\\phi_1\\w_2\\\phi_2\end{Bmatrix}=\begin{bmatrix}k_{11}&k_{12}&k_{13}&k_{14}\\k_{21}&k_{22}&k_{23}&k_{24}\\k_{31}&k_{32}&k_{33}&k_{34}\\k_{41}&k_{42}&k_{43}&k_{44}\end{bmatrix}\begin{Bmatrix}w_1\\\phi_1\\w_2\\\phi_2\end{Bmatrix}. \tag{19}$$

The inclusion of the stiffener, which is located between points 2^- and 2^+ in Fig. 3, is performed considering the transfer matrix relating the point 2^- with the point 2^+. Therefore, from Eq. (16),

$$w_2=w_{2^-}=w_{2^+}\quad\text{and}\quad\phi_2=\phi_{2^-}=\phi_{2^+} \tag{20}$$

$$V_2=V_{2^-}=V_{2^+}-\delta_1 w_{2^-}\quad\text{and}\quad M_2=M_{2^-}=M_{2^+}-\delta_2\phi_{2^-}. \tag{21}$$

Fig. 3. Spectral plate element including the effect of the reinforcement beam at node 2.

Substituting Eqs. (18) and (19) in Eq. (17), the dynamic stiffness element matrix relating points 1 and 2^+, which is the element matrix including the stiffeners, is given by

$$\begin{Bmatrix} V_1 \\ M_1 \\ V_{2^+} \\ M_{2^+} \end{Bmatrix} = \begin{bmatrix} k_{11} & k_{12} & k_{13} & k_{14} \\ k_{21} & k_{22} & k_{23} & k_{24} \\ k_{31} & k_{32} & k_{33}+\delta_1 & k_{34} \\ k_{41} & k_{42} & k_{43} & k_{44}+\delta_2 \end{bmatrix} \begin{Bmatrix} w_1 \\ \phi_1 \\ w_{2^+} \\ \phi_{2^+} \end{Bmatrix}. \tag{22}$$

Some special cases can be formulated using this methodology, the first case being when k_b and $k_e = 0$, Fig. 4. The terms are reduced to

$$\delta_1 = 2\left(\frac{E(I_b + Az_G^2)k_y^4 - \omega^2\rho A}{D}\right),$$
$$\delta_2 = 2\left\{\frac{GJ_bk_y^2 - \omega^2\rho I_p}{D(C + GJ_bk_y^2 - \omega^2\rho I_p)}\left[C + \omega^2\rho A\left(z_G - \frac{h}{2}\right)\frac{\Delta_2}{\Delta_1}\right] - \omega^2\rho Az_G\frac{\Delta_2}{\Delta_1}\right\}, \tag{23}$$

where, now, the area moments of the beams are computed with respect to their individual inertial centroid. The correction term for the beam thickness is made by the term in z_G, which is the distance between the beam centroid and the neutral plane of the plate. The expressions of $\Delta_{1,2}$ are given by

$$\Delta_1 = 1 - \frac{(z_G - (h/2))^2\omega^2\rho A}{C + GJ_bk_y^2 - \omega^2\rho I_p}, \quad \Delta_2 = \frac{h}{2} + \frac{C\left(z_G - (h/2)\right)}{C + GJ_bk_y^2 - \omega^2\rho I_p}. \tag{24}$$

Another case considered is when C is equal to ∞. The expressions for δ_1 and δ_2 are then reduced to

$$\delta_1 = 2(E(I_b + Az_g^2)k_y^4 - \rho A\omega^2),$$

$$\delta_2 = 2(GJk_y^2 - \rho I_p\omega^2) - 2\rho A\omega^2 z_g^2,$$

$$\Delta_1 = 1, \quad \Delta_2 = z_g.$$

Finally, assuming only one stiffener with $z_g = 0$,

$$\delta_1 = EI_bk_y^4 - \rho A\omega^2, \ \delta_2 = GJk_y^2 - \rho I_p\omega^2.$$

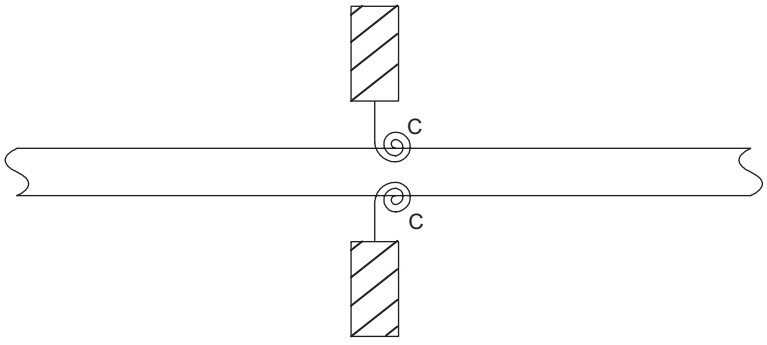

Fig. 4. Reinforcement beam with flexible connection to the plate (simplified model).

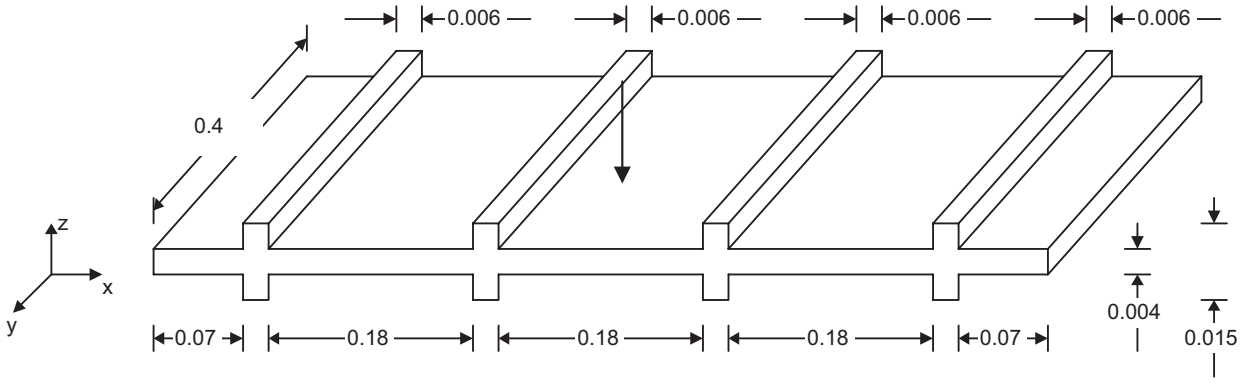

Fig. 5. Schematic diagram of the stiffened plate (units in meters).

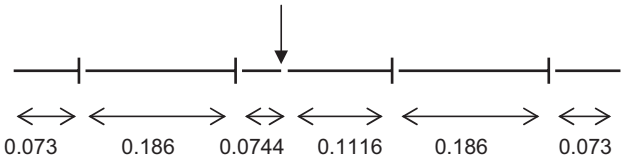

Fig. 6. Scheme of the spectral elements used in the model.

These terms are exactly the terms added to the spectral plate element to form the dynamic stiffness matrix of the reinforced plate element $[K_n] = [\beta_n][\alpha]^{-1}$ where $[\beta_n]$ is given in Eq. (14).

3. Verifying the spectral reinforced plate element

To verify the implementation of the spectral element reinforced plate element, a plate that is simply supported in the *yz*-plane and free–free in the *xz*-plane shown in Fig. 5 was modeled. The plate is assumed to have $E = 69\,\text{GPa}$, $\rho = 2700\,\text{kg/m}^3$, thickness $h = 4\,\text{mm}$, Poisson ratio $\upsilon = 0.3$, and dimensions $L_x = 700\,\text{mm}$, $L_y = 400\,\text{mm}$. Avoiding the main symmetry lines so that most of the modes can be excited, the driving point is arbitrarily located at position $(x, y) = (333.4{,}160)\,\text{mm}$. The receptances at the driving point for the spectral element model and finite element model solutions are compared. The spectral element model was evaluated using 4 reinforced plate and 2 simple plate elements as indicated in the scheme shown in Fig. 6. The response was obtained with 10 propagation modes for the frequency range DC-2 kHz, while the finite element model was implemented in Ansys® using shell63 elements, which have 4 nodes with 6 degree of freedom per node, and beam44 for the beam, totaling 18,180 nodes and 18,300 elements. The modal summation was made over 200 modes in order to obtain convergence of the receptance at the anti-resonances. Results obtained with the Fourier-series approach and image sources were not distinguishable from the sinusoidal solution using 40 Fourier lines. In Fig. 7 are shown the results obtained by the finite element and spectral element models (both methods practically coincide).

4. Computing the reflection and transmission coefficients

Defining a state vector for the plate cross-section at a given position x for pure bending as

$$X = \{w, \theta, M_{xy}, M_{xx}\}^{\mathrm{T}}, \tag{25}$$

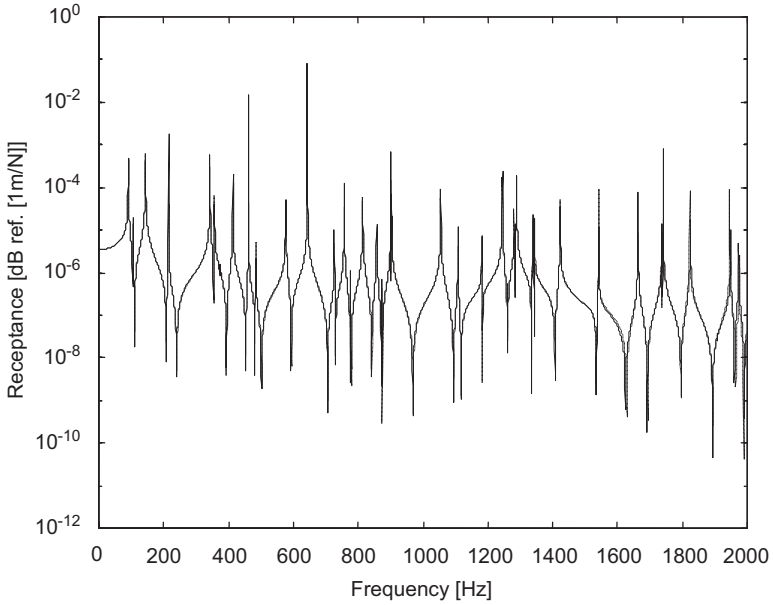

Fig. 7. Comparison of finite element (dashed) and spectral element model (continuous) results for the plate in Fig. 5. (Where the two curves are not distinguishable, it means that they match nearly exactly.)

the transfer matrix between 0^- and 0^+ can be written as in Eq. (16):

$$T(0^+,0^-)=\begin{bmatrix}1 & 0 & 0 & 0\\ 0 & 1 & 0 & 0\\ \delta_1 & 0 & 1 & 0\\ 0 & \delta_2 & 0 & 1\end{bmatrix}. \tag{26}$$

Combining the first two rows of Eqs. (5) and (6), we can write, for both 0^- and 0^+,

$$\begin{Bmatrix}w\\ \theta\\ V\\ M\end{Bmatrix}_{0^-,0^+}=\sin(k_y y)\begin{bmatrix}1 & 1 & 1 & 1\\ -\mathrm{i}k_1 & -k_2 & \mathrm{i}k_1 & k_2\\ \alpha_1 & \alpha_2 & -\alpha_1 & -\alpha_2\\ \beta_1 & \beta_2 & \beta_1 & \beta_2\end{bmatrix}\begin{Bmatrix}A\\ C\\ B\\ D\end{Bmatrix}=[\hat{E}]\begin{Bmatrix}A\\ C\\ B\\ D\end{Bmatrix}_{0^-,0^+}. \tag{27}$$

Given that the transfer matrix from x_{0^-} to x_{0^+} with a null length is given by Eq. (26), the matrix connecting the wave amplitudes before and after the discontinuity caused by the reinforcement beam is given by

$$\begin{Bmatrix}A\\ C\\ B\\ D\end{Bmatrix}_{0^+}=[\hat{E}]^{-1}\left[T(0^+,0^-)\right][\hat{E}]\begin{Bmatrix}A\\ C\\ B\\ D\end{Bmatrix}_{0^-}=\begin{bmatrix}G_{11} & G_{12}\\ G_{21} & G_{22}\end{bmatrix}\begin{Bmatrix}A\\ C\\ B\\ D\end{Bmatrix}_{0^-}. \tag{28}$$

The scattering matrix can be derived from Eq. (28) by re-arranging the terms:

$$\begin{Bmatrix}A_{0^+}\\ C_{0^+}\\ B_{0^-}\\ D_{0^-}\end{Bmatrix}=\begin{bmatrix}G_{11}-G_{12}G_{22}^{-1}G_{21} & G_{12}G_{22}^{-1}\\ -G_{22}^{-1}G_{21} & G_{22}^{-1}\end{bmatrix}\begin{Bmatrix}A_{0^-}\\ C_{0^-}\\ B_{0^+}\\ D_{0^+}\end{Bmatrix}=[S]\begin{Bmatrix}A_{0^-}\\ C_{0^-}\\ B_{0^+}\\ D_{0^+}\end{Bmatrix}. \tag{29}$$

The vectors $\{A_{0^+}\quad C_{0^+}\quad B_{0^-}\quad D_{0^-}\}^{\mathrm{T}}$ and $\{A_{0^-}\quad C_{0^-}\quad B_{0^+}\quad D_{0^+}\}^{\mathrm{T}}$ in Eq. (29) correspond to the amplitude vectors of the waves which are out-coming from the junction and to the amplitude vector of the

waves which are in-coming at the junction, respectively. The expressions for the reflection and transmission coefficients for purely propagative bending waves are then given by

$$\begin{aligned} T_{11} &= \{G_{11} - G_{12}G_{22}^{-1}G_{21}\}_{(1,1)}, \\ R_{12} &= \{G_{12}G_{22}^{-1}\}_{(1,1)}, \\ R_{21} &= \{-G_{22}^{-1}G_{21}\}_{(1,1)}, \\ T_{22} &= \{G_{22}^{-1}\}_{(1,1)}. \end{aligned} \tag{30}$$

Because of the symmetry properties of the scattering matrix, the absolute values of the reciprocal coefficients are equal, i.e., $|R_{12}| = |R_{21}|$ and $|T_{11}| = |T_{22}|$. In general, if no particular normalisation procedure is performed, phase discrepancies can exist between the coefficients and we do not have $R_{12} = R_{21}$ and $T_{11} = T_{22}$. Note that the reflection and transmission coefficients are functions of the frequency and of the wavenumber across the y direction, k_y. Given k_1 and k_y, the angle of incidence of an equivalent plane incident wave can be determined:

$$\tan(\theta) = \frac{k_y}{\sqrt{k_p^2 - k_y^2}} = \frac{n\pi/L_y}{\sqrt{(\omega^2\rho h/D)^{1/2} - (n\pi/L_y)^2}}. \tag{31}$$

The reflection and transmission coefficients apply to this incoming wave incidence angle. Ideally, the junction should be characterized by the wave reflection and transmission coefficients at an arbitrary frequency and angle of incidence. However, the wavenumber k_y takes the quantified values $n\pi/L_y$ imposed by the boundary conditions. Thus, it follows that at one given frequency the incidence angle is also quantified and takes the discrete values given by Eq. (31).

5. Measuring reflection and transmission coefficients

In order to simulate an experimental determination of the reflection and transmission coefficients at the reinforcement, the dynamic response of a plate was simulated and the incoming and outgoing complex wave amplitudes were computed from the transverse displacement measured at a few discrete locations on both sides of the reinforcing beam. The procedure was implemented such that it can be later applied to the experimental data. The physical model used to simulate an experiment is shown in Fig. 8. The locations where the response was simulated with the spectral element model are indicated. Where the dimensions are not given symmetry may be assumed.

In order to estimate the wave complex magnitudes from response measurements, the displacement field is assumed to obey an equation similar to Eq. (2) but with the evanescent terms neglected. This assumption imposes low frequency limits for the proposed experimental method. Furthermore, it is assumed that only the two first modes can propagate in the frequency range under consideration. A mode will propagate if k_{1n} is real. According to Eq. (3), this will depend upon the bending stiffness and mass density of the plate. Mode n is

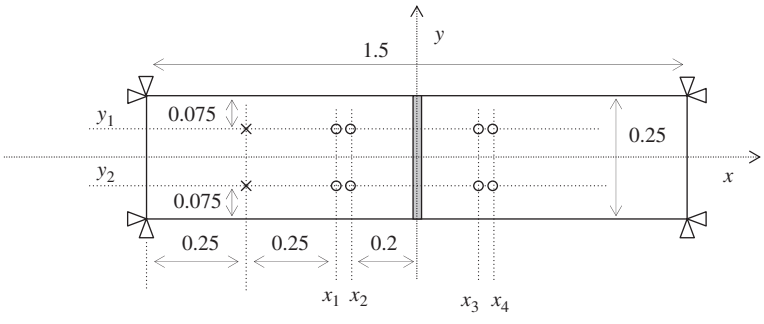

Fig. 8. Simply supported plate with reinforcing for determination of R and T coefficients.

propagating if

$$k_p^2 > k_{yn}^2. \tag{32}$$

This condition is equivalent to $f > f_n$, where $f_n = (1/2\pi)(n\pi/L_y)^2\sqrt{D/\rho h}$ is the cut-on frequency of mode n since it gives the minimum frequency value for mode n to propagate. For a given frequency range, the number of modes to consider can thus be determined by the number of cut-on frequencies in this range. Assuming a 10 mm-thick, 0.25 m large aluminum plate with material parameters $E = 67.5\text{E}9$, $\rho = 2800$ and $\upsilon = 0.33$, Eq. (32) gives a minimum frequency of 377.4 Hz for mode 1, 509.5 Hz for mode 2, and 3.396 Hz for mode 3. Limiting our range of analysis to 3.5 kHz, only modes 1 and 2 will significantly contribute to the response far from discontinuities. Therefore, we can write

$$w(x,y) \cong \sum_{n=1}^{2}\left[A_n e^{-ik_{1n}x} + B_n e^{ik_{n1}x}\right]\sin(k_{yn}y) = \sum_{n=1}^{2} Z_n \sin(k_{yn}y). \tag{33}$$

In order to determine the contribution of each mode, a linear system of equations may be assembled at each position along x using two measurements along y:

$$\begin{bmatrix} \sin(k_{y1}y_1) & \sin(k_{y2}y_1) \\ \sin(k_{y1}y_2) & \sin(k_{y2}y_2) \end{bmatrix}\begin{Bmatrix} Z_1 \\ Z_2 \end{Bmatrix} = \begin{Bmatrix} w(x,y_1) \\ w(x,y_2) \end{Bmatrix}. \tag{34}$$

In our case, the first mode, represented by a sinusoid along y, $\sin(\pi y/L_y)$, is symmetric with respect to a line passing through the mid-width of the plate (x-axis in Fig. 8), while the second mode is anti-symmetric, $\sin(2\pi y/L_y)$. Therefore, in order to decompose the responses into the two modes, it is sufficient to add two responses located symmetrically with respect to the x-axis to obtain the contribution of mode 1 and subtract them to obtain the contribution of mode 2. For arbitrary location of the measurements, the mode uncoupling can be done by solving Eq. (34). After separating the two modes, the complex amplitudes can be determined from Eq. (33) by assembling a linear system of equations, as shown in Eqs. (35) and (36):

$$\begin{bmatrix} e^{-ik_{11}x_1} & e^{ik_{11}x_1} \\ e^{-ik_{11}x_2} & e^{ik_{11}x_2} \end{bmatrix}\begin{Bmatrix} A_{0-} \\ B_{0-} \end{Bmatrix}_{\text{mode1}} = \begin{Bmatrix} Z_1(x_1) \\ Z_1(x_2) \end{Bmatrix} = \begin{Bmatrix} [w(x_1,y_1)+w(x_1,y_2)]/2 \\ [w(x_2,y_1)+w(x_2,y_2)]/2 \end{Bmatrix}, \tag{35}$$

$$\begin{bmatrix} e^{-ik_{12}x_1} & e^{ik_{12}x_1} \\ e^{-ik_{12}x_2} & e^{ik_{12}x_2} \end{bmatrix}\begin{Bmatrix} A_{0-} \\ B_{0-} \end{Bmatrix}_{\text{mode2}} = \begin{Bmatrix} Z_2(x_1) \\ Z_2(x_2) \end{Bmatrix} = \begin{Bmatrix} [w(x_1,y_1)-w(x_1,y_2)]/2 \\ [w(x_2,y_1)-w(x_2,y_2)]/2 \end{Bmatrix}. \tag{36}$$

Similar equations can be written for the measurements on the positive side of the x-axis, so that complex amplitudes can be computed at the two sides of the reinforcing beam:

$$\begin{bmatrix} e^{-ik_{11}x_3} & e^{ik_{11}x_3} \\ e^{-ik_{11}x_4} & e^{ik_{11}x_4} \end{bmatrix}\begin{Bmatrix} A_{0+} \\ B_{0+} \end{Bmatrix}_{\text{mode1}} = \begin{Bmatrix} [w(x_3,y_1)+w(x_3,y_2)]/2 \\ [w(x_4,y_1)+w(x_4,y_2)]/2 \end{Bmatrix}, \tag{37}$$

$$\begin{bmatrix} e^{-ik_{12}x_3} & e^{ik_{12}x_3} \\ e^{-ik_{12}x_4} & e^{ik_{12}x_4} \end{bmatrix}\begin{Bmatrix} A_{0+} \\ B_{0+} \end{Bmatrix}_{\text{mode2}} = \begin{Bmatrix} [w(x_3,y_1)-w(x_3,y_2)]/2 \\ [w(x_4,y_1)-w(x_4,y_2)]/2 \end{Bmatrix}. \tag{38}$$

The linear system of Eq. (29) can be rearranged, with $R_{12} = R_{21} = R$; $T_{11} = T_{22} = T$, as

$$\begin{bmatrix} A_{0-} & B_{0+} \\ B_{0+} & A_{0-} \end{bmatrix}\begin{Bmatrix} T \\ R \end{Bmatrix} = \begin{Bmatrix} A_{0+} \\ B_{0-} \end{Bmatrix} \tag{39}$$

and be solved for R and T. All these operations must be performed for each mode and for each frequency.

The spectral element model for the plate in Fig. 8 could be assembled with as little as 3 spectral elements, as the discontinuities along x are only the excitation location and the reinforcing beam. However, given that the model is so simple, in order to avoid having to interpolate the responses from the nodal responses, 7 elements were used so that each measurement location is a node of the model.

Thinking about practical experimental problems to be faced later, two excitation configurations were used. In the first configuration the two excitation locations, indicated in Fig. 8 by crosses, are in-phase, so as to enhance the contribution of the first mode, while, in the second configuration, they are out-of-phase, to excite the second mode. In the theoretical data, the symmetry of the problem would allow an exact uncoupling using Eqs. (34) and (39), but, in the experimental case, symmetry is not exact, and enhancing modal response is important. Otherwise, mode extraction can be improved using more measurement points and solving the problem in a least-squares sense.

Another problem in the calculation of R and T is the possible ill-conditioning of Eqs. (34) and (39) when the vibration field is too reverberant (low damping). In order to improve conditioning and simulate an experiment where sand boxes are used to damp vibrations at the plate ends, damped springs were added to the simple supports at $x = \pm 0.75$ m. It is straightforward to do so in the model simply by adding a complex stiffness to the diagonal elements of the global dynamic stiffness matrix at the locations corresponding to the desired degrees of freedom. In our example, the complex value added to the rotational degrees of freedom corresponding to the two simple supports at the plate ends was $500 + 10i$.

Two reinforcing beams placed on either side of the plate with cross-section 0.02 mm $\times$ 0.02 mm, made of the same aluminum as the plate, were simulated. Results are shown in Figs. 9 and 10 for connecting stiffness parameters $\alpha = 0.25$, $C = 1e6$ N m/rad, $k_e = 7e8$ N/m, $k_b = 1e9$ N/m for mode 1. When obtaining results for mode 2, the transverse connection bending stiffness was changed to $k_b = 1e8$ N/m, as it is expected that the bolted connection that will be implemented in the experiment will behave differently for these two different modes. The exact R and T curves can be obtained with Eq. (30) and compared with the values computed from the simulated responses using the methodology described above.

At low frequencies, below the frequency above which the mode can propagate, it is expected that the method proposed for computing R and T from a few discrete point responses will not work, as there are only

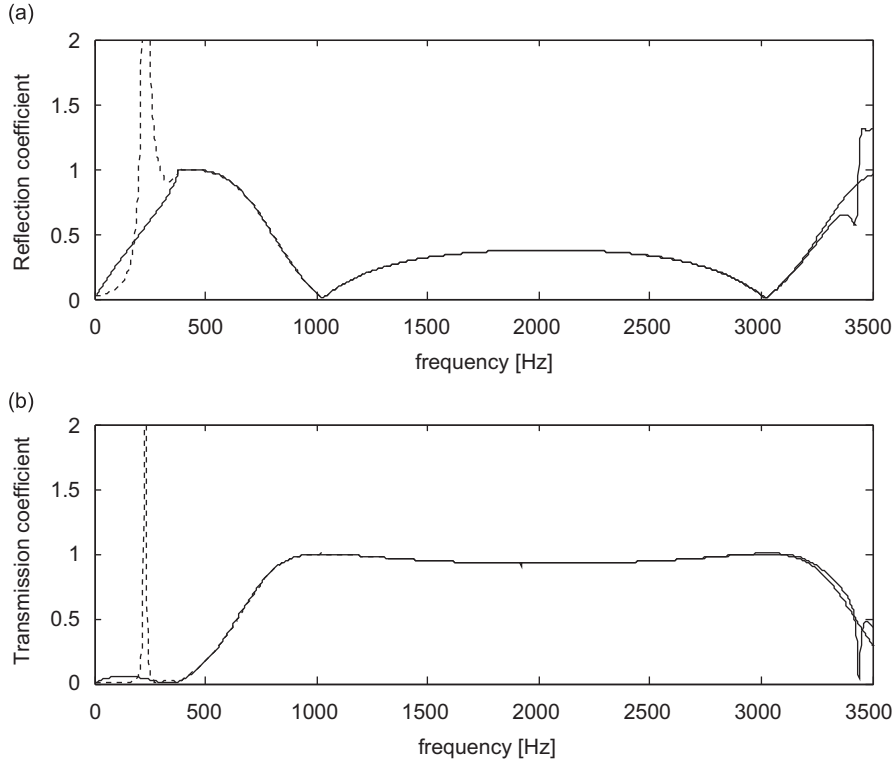

Fig. 9. Reflection (a) and transmission (b) coefficients for mode 1 ($f_n = 377$ Hz). —Theoretical and - - - computed from spectral element model. (Where the two curves are not distinguishable, it means that they match nearly exactly.)

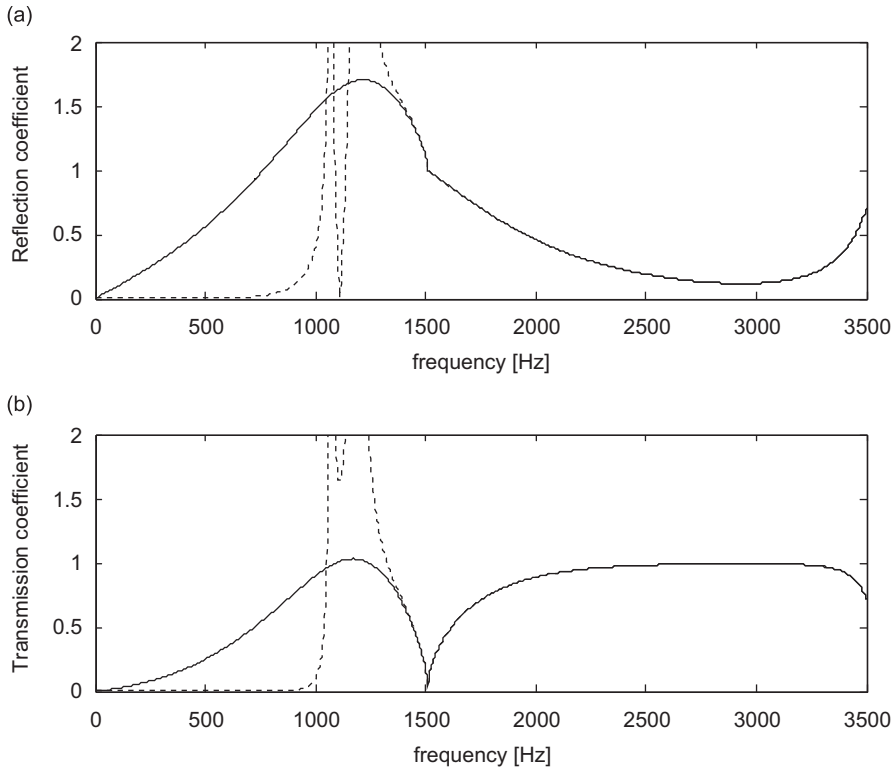

Fig. 10. Reflection (a) and transmission (b) coefficients for mode 2 ($f_n = 1509$ Hz). —Theoretical and - - - computed from spectral element model. (Where the two curves are not distinguishable, it means that they match nearly exactly.)

evanescent waves, and even the concept of reflection and transmission coefficients is lost. Results below the cut-off frequency can therefore be disregarded.

6. Conclusions

The possibility of obtaining reflection and transmission coefficients for bending waves in thin plates caused by a reinforcing beam that is flexibly connected to the plate was investigated. For this purpose, a reinforced plate spectral element was derived and implemented. A system consisting of a simply supported long rectangular plate, treated here as a wave-guide, was numerically simulated using a spectral element model, and the dynamic responses at a few locations were used to compute the reflection and transmission coefficients. The choice of the lateral boundary conditions for the plate is mainly due to the fact that this is a simple way to quantify the transverse wavenumber and thus to control the incidence angle of the flexural wave. In order to derive the theoretical expressions of the coefficients, the transfer matrix of the plate and of the beam alone were derived. The coefficients obtained by using the proposed method were compared with the theoretical values and a very good agreement was found, thus validating the proposed technique. The numerical model can be used to optimize the experimental conditions for extracting the reflection and transmission coefficients. The reflection and transmission coefficients obtained this way can be used to characterize a given reinforcement beam flexibly connected to a thin plate in a ribbed panel assembly.

The limitations of the proposed method should be pointed out. Ideally, the junction should be characterized by the reflection and transmission coefficients at an arbitrary frequency and angle of incidence. However, measurements are only possible for quantified values of the incidence angle, which are imposed by the quantified values of the transverse wavenumber. From a practical point of view, the main difficulties of the method are linked to the technical realization of the simply supported boundary conditions. If the simply

boundary conditions are not well satisfied, transverse propagation modes of the wave-guide are not sinusoidal and the determination of the reflection and transmission coefficients becomes much more difficult. It should be pointed out that, even when simply supported boundary conditions are well satisfied, accurate separation of the lateral modes remains an important practical difficulty, which can be overcome by increasing the number of measurement points. Even with the present limitations, the method can be useful for the determination of R and T for complex joints. It is well known that joints in built up structures are difficult to model and to characterize. Such coefficients can be used in ray-tracing methods applied to structures, which are currently under development.

Acknowledgments

The authors are thankful to the Brazilian funding agencies FAPESP, CNPq, and CAPES and to the French CNRS for the financial support.

References

[1] R.H. Lyon, R.G. Dejong, *Theory and Application of Statistical Energy Analysis*, second ed., Butterworth-Heinemann, London, 1995.
[2] K.S. Chae, J.G. Ih, Prediction of vibrational energy distribution in the thin plate at high frequency bands by using the ray tracong method, *Journal of Sound and Vibration* 240 (2) (2001) 263–292.
[3] L. Cremer, M. Heckl, *Structure-borne Sound*, second ed., Springer, Berlin, 1972.
[4] M. Heckl, Wave propagation on beam–plate system, *Journal of the Acoustical Society of America* 33 (5) (1961) 640–651.
[5] E.E. Ungar, Transmission of plate flexural waves through reinforcing beams; dynamic stress concentration, *Journal of the Acoustical Society of America* 33 (5) (1961) 633–639.
[6] N.J. Kessissoglou, J. Pan, An analytical investigation of the active attenuation of the plate flexural wave transmission through a reinforcing beam, *Journal of the Acoustical Society of America* 102 (6) (1997) 3530–3541.
[7] D.P. Kouzov, T.S. Kravtsova, Vibrational mode conversion in a plate at a reinforcing beam, *Soviet Physics Acoustics* 29 (2) (1983) 118–122.
[8] T. Balendra, N.E. Shanmugam, Free vibration of plated structures by grillage method, *Journal of Sound and Vibration* 99 (3) (1985) 333–350.
[9] D.J. Mead, A.K. Mallik, An approximate theory for the sound radiated from a periodic line-supported plate, *Journal of Sound and Vibration* 61 (3) (1978) 315–326.
[10] R.F. Keltie, Structural acoustic response of finite rib-reinforced plates, *Journal of the Acoustical Society of America* 94 (2) (1993) 880–887.
[11] M.C. Junger, D. Feit, *Sound, Structures, and Their Interaction*, Acoustical Society of America, 1993.
[12] B.R. Mace, Sound radiation from a plate reinforced by two sets of parallel stiffeners, *Journal of Sound and Vibration* 71 (3) (1980) 435–441.
[13] B.R. Mace, Periodically stiffened fluid-loaded plates. I: response to convected harmonic pressure and free wave propagation, *Journal of Sound and Vibration* 73 (4) (1980) 473–486.
[14] D.J. Mead, Wave propagation in continuous periodic structures: research contributions from Southampton, 1964–1995, *Journal of Sound and Vibration* 190 (3) (1996) 495–524.
[15] R.S. Langley, K.H. Heron, Elastic wave transmission through plate/beam junctions, *Journal of Sound and Vibration* 143 (2) (1990) 241–253.
[16] V. Zalizniak, Y. Tso, L.A. Wood, Waves transmission through plate and beam junctions, *International Journal of Mechanical Sciences* 41 (1999) 831–843.
[17] G. Pavic, Measurement of energy properties of mechanical joints using a standard Oberst apparatus, *Proceedings of International Conference NOVEM 2000*, 31 August–2 September 2000, INSA de Lyon, Lyon, France.
[18] L. Feng, M. Liu, A. Nilsson, Experimental study of structure-borne sound transmission of mechanical joints, *Journal of the Acoustical Society of America* 110 (3, Part 1) (2001) 1391–1397.
[19] F. Gautier, M.H. Moulet, J.C. Pascal, Scattering matrix of a stiffener elastically connected to a plate, *Proceedings of the International Conference on Recent Advances in Structural Dynamics*, Southampton, UK, 2003.
[20] J.F. Doyle, *Wave Propagation in Structures: Spectral Analysis Using Fast Discrete Fourier Transforms*, second ed., Springer, New York, 1997.
[21] U. Lee, J. Lee, Spectral-element method of Levy-type plates subjected to dynamic loads, *Journal of Engineering Mechanics* (1999) 243–247.
[22] P.H. Kulla, High precision finite elements, *Finite Elements in Analysis and Design* 26 (2) (1997) 97–114.
[23] R.J. Craig, *Structural Dynamics: An Introduction to Computer Methods*, Wiley, New York, 1981.